Chemical Papers (2021) 75:297–309
https://doi.org/10.1007/s11696-020-01299-8

ORIGINAL PAPER

Synthesis, structural characterization, DFT, kinetics and mechanism of oxidation of bromothymol blue: application to textile industrial wastewater treatment

Samia M. Ibrahim[1] · **Ahmed F. Al-Hossainy**[1,2]

Received: 18 May 2020 / Accepted: 25 July 2020 / Published online: 4 August 2020

Abstract

Oxidation of bromothymol blue [BTB] by oxyanion potassium permanganate as a strong oxidizing agent in acid solutions using perchloric acid at a constant ionic strength has been obtained keto bromothymol blue $[BTB]^{Keto}$ and studied kinetically spectrophotometrically. Different characterization techniques for [BTB] and $[BTB]^{Keto}$ such as Fourier-transform infrared spectroscopy (FTIR), ultraviolet–visible spectroscopy (UV–Vis), and optical properties have been used. The order about the permanganate ion is first, while a fractional first order was released as regards $[H^+]$ and [BTB] fractional first order. Dependence on the concentration of hydrogen ions in the concentrations indicates that the oxidation process is acid catalyzed. The absence of either transient Mn^{III} and/or Mn^{IV} as involving species in the oxidation process was verified by Mn^{II} applied to the oxidation reaction. Formation of 1:1 intermediate complex formation kinetically was revealed during the rate-determination step. In the slowest step, two-electron transfer processes of the inner-sphere form have been proposed. A mechanism of the tentative reaction was proposed and explored concerning kinetic parameters. The density functional theory (*DFT*) by *DMol*^{3} and *CASTEP* was used for the optimization of dye [BTB] and $[BTB]^{Keto}$ as an isolated molecule. From the UV–Vis spectrum of [BTB] and $[BTB]^{Keto}$, the E^{Opt}_{Direct} values are 2.849 eV and 2.35 eV using *Tauc`s* equation, respectively, related to direct transitions of electrons. Using *DMol*^{3} method with *DFT* simulation, the HOMO and LUMO values for [BTB] and $[BTB]^{Keto}$ as isolated molecule are 3.047 eV and 2.869 eV, respectively. The simulated FTIR, molecular electrostatic potential (MEP) and optical properties by *Gaussian software* and *CATSTEP* are in great agreement with the experimental study.

Graphic Abstract

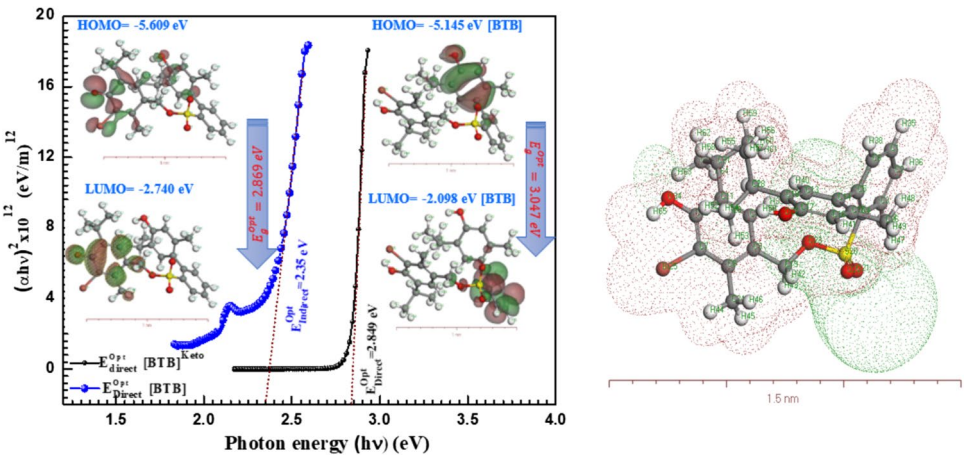

Keywords Keto bromothymol blue · Oxidation · Kinetics mechanisms · Energy gap · DFT calculation

Extended author information available on the last page of the article

Introduction

The textile industry is one of the largest water-consuming industries (Rashid et al. 2020). They refuse large amounts of wastewater. Such wastewaters contain toxic dyes and pigments that have a negative influence on human health and the ecosystem (Khan and Malik 2014). The existence of dyes in wastewater creates various hazards for living organisms, such as mutagens and carcinogenic problems, and reduces photosynthesis; by limiting the penetration of oxygen into water (Saini 2017). Multiple methods treat these effluents (Gao et al. 2020). However, in the presence of toxic and non-biodegradable dyes, the biological treatments are ineffective and produce high quantities of sludge; the physicochemical methods do have a high investment cost (Badeenezhad et al. 2019). These limitations mean that new efficient processes are developed. A photocatalytic solution for wastewater polluted by color bleeding from fabric, rubber, natural and artificial fabrics. Bromothymol blue (BTB) is a silk dye product often used as the pH measure (Li et al. 2018). It is a useful probe molecule that is not corrupted by direct oxidation and can only be chemically degraded via free-radical pathways.

The strong oxidizing agent ($KMnO_4$) has some advantages over other oxidizing agents: easier to handle, a readily soluble solid and higher performance in water and soil treatment as seen with some pollutants (Xu et al. 2005). Permanganate ion is an effective oxidant in acid, neutral and basic media that is known to be a leading, environmentally friendly, and active oxidant in kinetic research (Liu et al. 2019). Oxidation by permanganate ion have a various mechanism so, permanganate ion is used as a multi-equivalent oxidant (Hassan 2020). The mechanism of some redox reactions was focused on intermediate complexes (Al-Hossainy and Zoromba 2019) production, whereas free-radical mechanisms (Tittmann 2009; Mollan and Alayash 2013) studied other redox reactions. Methylcellulose kinetics and oxidation mechanism (Shaker et al. 2007; Hassan 1993), alginates (Khairou and Hassan 2000), pectates (Shaker 2001), carboxymethyl cellulose (Hassan et al. 2011), kappa-carrageenan (Zaafarany et al. 2013), and polysaccharides of permanganate ion have been recorded elsewhere in alkaline media. Again, the oxidation of methylcellulose (Hassan et al. 2012), pectates (Abdel-Hamid et al. 2003), carboxymethyl cellulose (Hassan et al. 2009a), carrageenan's (Hassan et al. 2009b), ADA (Hassan and Ibrahim 2019a), poly (ethylene glycol) (Hassan et al. 2018a) and chondroitin-4-sulfate (Hassan et al. 2020a) by permanganate ion in acidic solutions has been reported earlier. Pseudo-first-order plots were shown to be reversed S-forms in these oxidation reactions and free radical interference carried out the oxidation reactions.

Previous studies have neglected to consider the effects of $KMnO_4$ as an oxidizing agent on the structure characterization, spectroscopic studies, and optical properties of dye [BTB]. In this work, the decoloration of the BTB coloring solutions by $KMnO_4$ was investigated kinetically. Effects of pH, reactant concentration and decoloration temperature have been studied. The application of $KMnO_4$ for the treatment of real textile wastewater was also carried out. The present work seems to merit a study to shed more light on the mechanistic aspects of oxidation and to cover for the lack of information on the existence of both the electron transfer and the transition states in the rate-determining phase. The results obtained will offer important knowledge on the chemistry of BTB dye as one of the sulfones phthalein's in acidic solutions. Again, this study will boost the elucidation of an appropriate oxidation reaction process in acidic solutions for these alcoholic dyes. Once more, in this work besides the oxidation of BBT we used the unified coverage $DMol^3$ obtained from molecular to solid materials is discussed briefly. So, molecules in the gas state are pertinent for the properties of molecular materials and homogeneous catalysis reactions. In comparison studies between experimental and *DFT* computations, the structural characterization, and optical properties of [BTB] and $[BTB]^{Keto}$ were examined utilizing characterization techniques comprising Fourier transform infrared (FTIR).

Experimental section

Materials

All used products are analytical grade. Water has doubly been distilled from alkaline permanganate and degassed through the atmospheric pressure bubbling, boiling, and cooling (Manhas and Mohammed 2007). Through adding the reagent powder to double distilled water step through process, [BTB] (Aldrich Chemical Co. Ltd) solutions in stock was prepared and the solution rapidly was agitated. A $KMnO_4$ stock solution has been prepared and standardized using traditional methods (Bahar et al. 2020). The stock solution was then placed in a dark container away from light to prevent photoreduction and was spectrophotometrically re-standardized before each use. By dissolving the required sample amounts in double distilled water, all other reagents were prepared. The ionic strength was kept in check by the addition of $NaClO_4$ as non-complexing agent (Hassan et al. 2020b; Tandon et al. 2007). In ± 0.05 °C, the temperature was regulated.

Kinetic measurements

The present oxidation reaction for the available spectrophotometer was relatively quick. All kinetic operations

have been made under the scope of pseudo-first-order (Hassan and Ibrahim 2019b; Hicks 1976; Hassan et al. 2018b). The absorption decrease was recorded at 525 nm at permanganate ion, with the maximum absorption depending on time (where [BTB] > 10 $[MnO_4^-]^0$). During the reaction process, no overlaps were found with other [BTB], MnO_4^- and substances at this wavelength. As Fig. 1a indicates, an isosbestic point is found at a wavelength of 274 nm. Once, a new strip at a wavelength of around 380 nm was used to produce the permanganate ion of the same concentration of the mixture being studied (Fig. 1b). These observations may indicate the formation of some intermediate complexes.

Absorbance–time plots revealed that the initial component (~ 5–10%) was too quick for the traditional spectrophotometer to be followed. Therefore, the kinetic calculations listed concerned the remaining portion of the completion of the reaction (~ 90–95%). In the presence of a large quantity [MnO_4^-] above [BTB] in all kinetic measurements pseudo-first-order conditions were used. Sodium perchlorate, $NaClO_4$, used as an inert electrolyte to maintain ionic strength constant. The absorbance shift measurements on the spectrophotometer Perkin Elmer (Lambada 750) with a thermostat cell partition using a path length of cells of 1 cm in total. The estimation method was the same as elsewhere (Manhas and Mohammed 2007). Figure 1a, b indicates the spectral variations during the redox reaction.

Polymerization test

Ten percent acrylonitrile (v/v) has been used in the reaction mixture during oxidation; to test the possibility of free radical's formation brown forming after 15 min of warmth indicates the oxidation reaction by free-radical interference process (Ibrahim et al. 2017; Laidler 1965a; Hassan et al. 2013). Again, the same observation occurs when we replaced acrylonitrile by mercuric chloride.

Molecular modeling

The structure molecular, spectral simulation and geometry optimization for [BTB] and $[BTB]^{Keto}$ as isolated molecular have been elucidated in detail by analysis of an Infrared (IR) combined with *Gaussian 09 W program* (Abdel-Aziz et al. 2020). In IR calculation using the *Gaussian 09 W (DFT/B3LYP)*, the functional exchange–correlation level demonstrates the wavenumber and the location of functional groups in [BTB] and $[BTB]^{Keto}$ as isolated molecular (Pavitha et al. 2017; Bourezgui et al. 2020). Finally, the optical characterization and optical constant have been elucidated in detail by analysis of *DMOl*^{3} and *CATSTEP* computations. Using *Gauss View software*, the HOMO and LUMO values have been computed in detail by analysis of UV–Vis spectrum using *DFT/DMOl*^{3} by typical *6–311G* set of bases (Srebro et al. 2011; Zoromba and Al-Hossainy 2020).

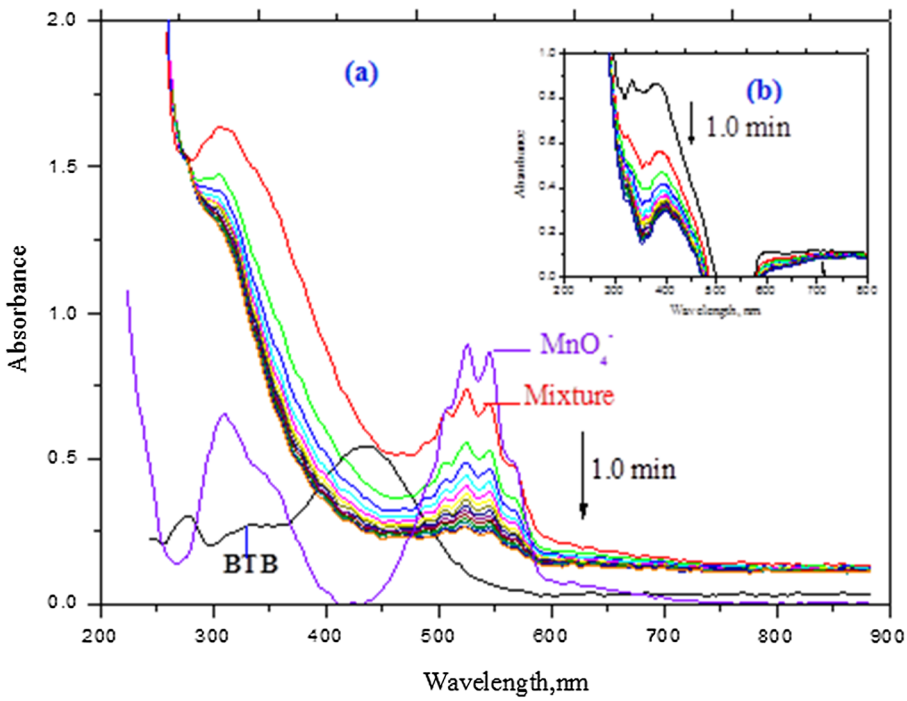

Fig. 1 Spectral dependence of the absorption in the oxidation of [BTB] by [MnO_4^-] in aqueous $HClO_4$ during the reaction progression. **a** $[MnO_4^-] = 4.0 \times 10^{-4}$, $[BTB] = 1.0 \times 10^{-3}$, $[HClO_4] = 0.5$ and $I = 1.0$ mol dm^{-3} at 20 °C. Scanning time intervals = 1.0 min. **b** $[MnO_4^-] = 4.0 \times 10^{-4}$, $[BTB] = 1 \times 10^{-3}$, $[H^+] = 0.5$ and $I = 1.0$ mol dm^{-3} (Reference cell: $[MnO_4^-] = 4.0 \times 10^{-4}$ mol dm^{-3} at 20 °C)

Results

Stoichiometry

The oxidation reaction with varying initial [BTB] and $[MnO_4^-]$ concentrations was combined at room temperature at $[H^+] = 0.5$ and I = 1.0 mol dm^{-3}. The unreacted permanganate ion is expected to reach a constant value regularly. There has been a stoichiometric average of 1.0 mol ($[MnO_4^-]$ unreacted /$[BTB]^0$). The corresponding stoichiometric equation is agreed with

$$C_{27}H_{28}Br_2O_5S + MnO_4^- + 4H^+ \rightleftharpoons C_{27}H_{24}Br_2O_5S + Mn^{2+} + 4H_2O \quad (1)$$

where $C_{27}H_{28}Br_2O_5S$ and $C_{27}H_{24}Br_2O_5S$ represent the [BTB] and $[BTB]^{Keto}$, respectively. The $[BTB]^{Keto}$ had been isolated by another approach (Hassan et al. 2019).

The product was also recognized by the FTIR spectral bands detected at frequency 3448 cm^{-1} and 3443 cm^{-1} that characterize the two –OH groups in [BTB] and these two bands converted to one band at 3443 cm^{-1} so, this confirms the oxidation occurs at one –OH group (Abd-Elmageed et al. 2020; Xu et al. 2020; Surowka et al. 2020; Al-Hossainy et al. 2019a). Moreover, band observed at 1720 cm^{-1} that characterize the carbonyl group of α-ketones; strong band appear at 2962 cm^{-1} which characterize CH_2 group in case of [BTB] but appear weak band at 2962 cm^{-1} in case of $[BTB]^{Keto}$ which characterize –CH group (Zoromba et al. 2018). Enhancing the OH group absorption band at a wavelength of 1720 cm^{-1} in the product's IR spectra can show oxidation of the OH group present in [BTB] dye to its corresponding keto-forms as display in Fig. 2a (Rauf et al. 2015).

In the simulated IR spectrum of [BTB] (Fig. 2b), the band at 3600 cm^{-1} bands disappeared in the $[BTB]^{Keto}$ in Fig. 2c spectrum. This is attributed to stretching hydroxyl group ν(O–H) present in benzene oxidized to ketone group and formation $[BTB]^{Keto}$ dye. It is essential to note that the experimental curve shows great conformity with *Gaussian 09 W (DFT/B3LYP)* simulation (Thabet et al. 2020; Farzaneh et al. 2020; Ibrahim et al. 2020; Abbasi and Sardroodi 2016). Especially, 3750 cm^{-1}.

Influence of reaction rate on $[MnO_4^-]$ and [BTB]

ln (absorbance) against time, plots showed that the redox reaction in MnO_4^- is first in a sequence, with well straight lines for more than two half-lives of end reaction. Not only pseudo plotting but also an independently of the oxidation rates at different initial permanganate concentrations ranging from 1×10^{-4} to 5×10^{-4} mol dm^{-3} have confirmed this effect. The influence of [BTB] on the oxidation rates has been investigated. The values of oxidation rate were found to increase with increasing the [BTB]. So, these values at [BTB] = (1.0 and 3.0) $\times 10^{-3}$ mol dm^{-3} were found to be (0.58 and 1.47) $\times 10^{-3}$ s^{-1}, respectively. A fractional-first-order in [BTB] was obtained from the plots of ln k_{obs} and ln[BTB] and is confirmed by (ln $k_{obs} = n$ ln [BTB] equation). Once more, straight lines were achieved by drawings of $1/k_{obs}$ in the $HClO_4$ positive intercept axis on an *X*-axis against 1/[BTB]. The present redox system shows the creation of 1:1 intermediate complex shown by Michaelis–Menten kinetics (Fig. 3). The naked eye examination of the mixture revealed that the purple color of the permanganate ion in the mixture was modified to the orange color which changes rapidly to the rose color as shown in inset Fig. 3.

Influence of reaction rate on hydrogen ion concentrations

To explain the reaction rate and evaluate the successful reaction mechanism, $[H^+]$ controlled the constant ionic strength of 1.0 mol dm^{-3} and the constant concentrations of all other reagents. There was a rise in the acid amount to speed up the rates of oxidation and then the values of the rate constants at $[H^+] = 0.5$ and 1.0 mol dm^{-3} were found to be 0.58×10^{-3}, 1.51×10^{-3} s^{-1}, respectively. The oxidation reaction is therefore catalyzed acidically. Dependence from $[H^+]$ was fractional first order (ln k_{Obs} – ln $[H^+]$ plots).

Influence of reaction rate on ionic strength

The effect of the ionic strength was studied in constant $[H^+]$ reaction levels with the rise of $NaClO_4$ concentration to 1.5 mol dm^{-3}. This result was found to fit the extended Debye–Huckel equation (ln k_{Obs} vs. $\frac{\sqrt{I}}{1+\sqrt{I}}$ plot) with a positive slope as shown in Fig. 4. The dependence of ionic strength is as expected in consideration of the charges, despite the ionic strength used, far from the Debye–Huckel range (Laidler 1965b). The oxidation reaction between a neutral and cation molecule can therefore occur.

Reaction rate impact on salts added

The oxidation rate effect of Mn^{2+} must be studied as it is one of the oxidation materials is indicated that Mn^{2+} is reduced to Mn^{III} and Mn^{IV} as a transient species (Radhakrishnamurti and Rao 1977; Gunter et al. 2010).

Where reactive oxidizing species are intermediates of Mn^{III} and/or Mn^{IV}, the addition of Mn^{II} will lead in the oxidation rate accelerations. While, fluoride ions should slow down the reaction if manganese ions are primarily the oxidation responsible species, but if permanganate ions are the primary oxidizing entities, they should not be significantly altered (Knežević et al. 2020). In addition to

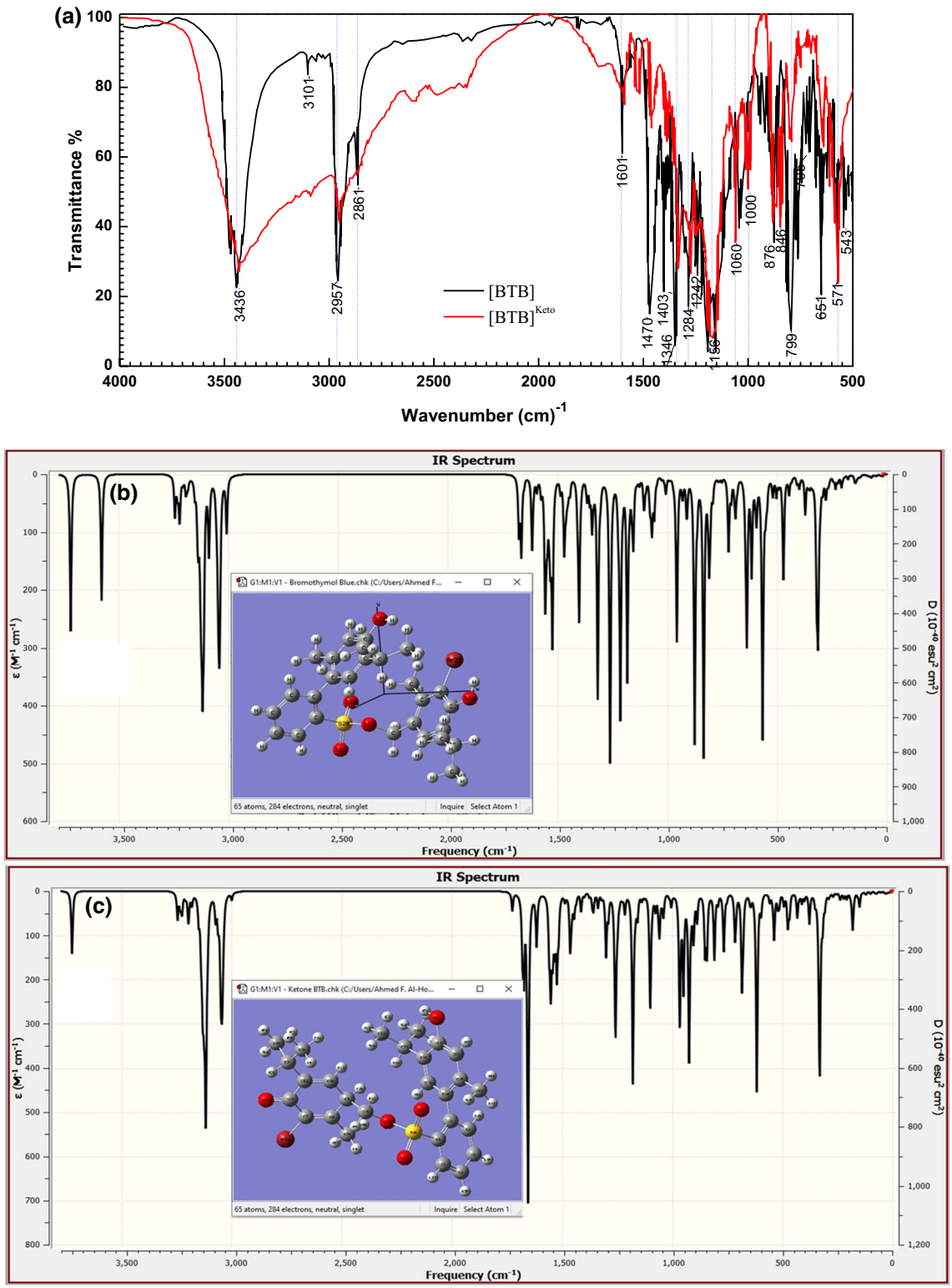

Fig. 2 **a** FTIR spectrum experimental of [BTB] and $[BTB]^{Keto}$. **b** IR spectrum of [BTB] using DFT simulation. **c** IR spectrum of $[BTB]^{Keto}$ using *Gaussian 09 W (DFT/B3LYP)* simulation

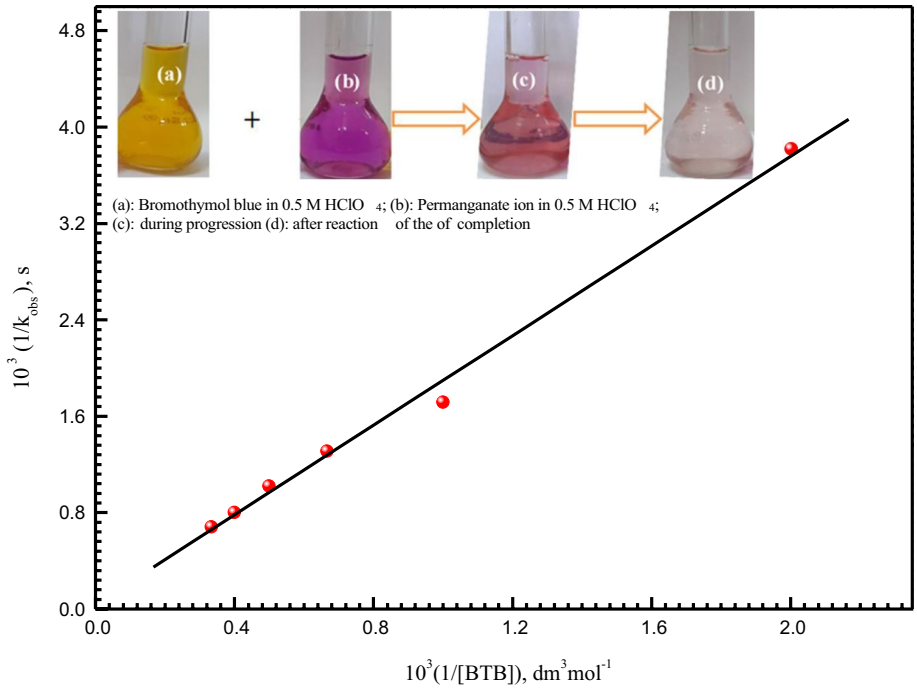

Fig. 3 Chart $1/k_{obs}$ against 1/[BTB] in perchlorate solutions to oxidize [BTB] through permanganate ion. $[MnO_4^-]=4.0\times10^{-4}$, $[H^+]=0.5$ and $I=1.0$ mol dm^{-3} at 35 °C. Inset figure, Naked eye examination for color shift **a**: BTB in 0.5 M $HClO_4$; **b**: MnO_4^- in 0.5 M $HClO_4$; **c**: during progression, **d**: after reaction of the of completion

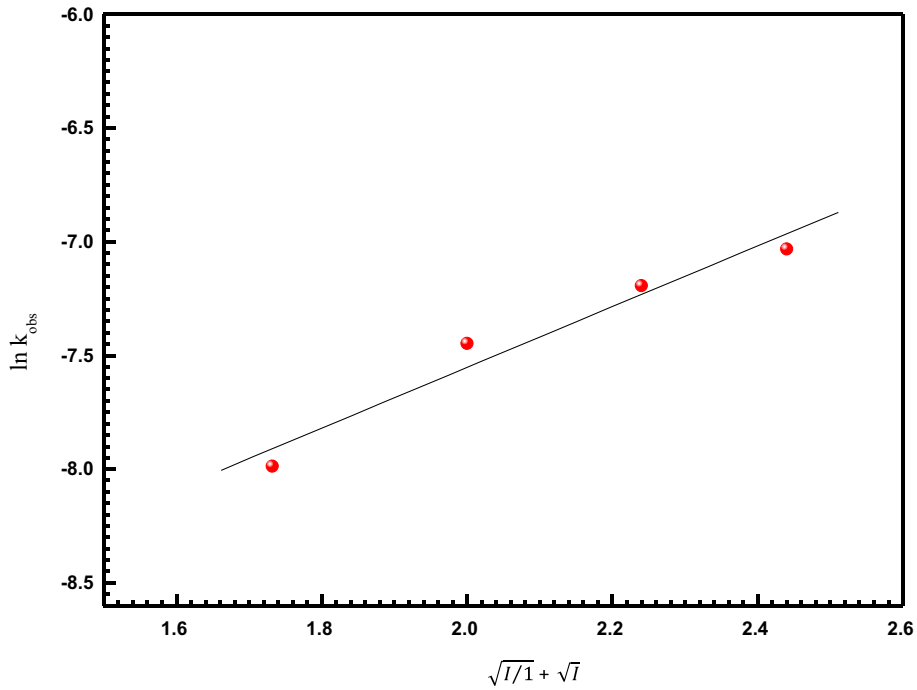

Fig. 4 The relationship between $t\sqrt{I}/\left(1+\sqrt{I}\right)$ versus $\ln k_{Obs}$ of [BTB] by $[MnO_4^-]$ in $HClO_4$ solutions. $[MnO_4^-]=4.0\times10^{-4}$, $[BTB]=1.0\times10^{-3}$, $[H^+]=0.5$ mol dm^{-3} at 35 °C

the redox reaction, either $[Mn^{II}]$ or $[F^-]$ ions were found to have no significant changes in the reaction rates under our experimental conditions. This negative outcome can be perceived as suggesting the absence of Mn^{III} or Mn^{IV} formation as transient material intermediates in the oxidation reaction.

Discussion

Although there has been substantial research on the kinetics of oxidation by permanganate ion of organic, inorganic substrates and alcoholic macromolecules in acidic solutions as multi-equivalent oxidants, several unanswered

questions concerning the mechanisms of oxidation in terms of electron transfer and the intermediate states in the rate-determining processes have been recorded (Wasserman et al. 2016). Therefore, there may be a problem of fundamental importance, whether the transition, in a series or the simultaneous two-electron transitions, of electrons, takes place through a sequential one-electron transfer procedure: Mn^{VII} to Mn^{VI} to Mn^{V} in a sequence or Mn^{VII} to Mn^{V} to Mn^{III} in a single step.

Therefore, it is important to know whether the pathways for the process of electron transfer outer-sphere or inner-sphere type. The complexity of the reactions concerning the formation of unstable intermediates by the transfer of manganese ions from heptavalent to divalent in acidic solutions will cause these difficulties. Consequently, this oxidant has proposed different reaction pathways for the oxidation of various substrates. Many redox reactions tend to take place by free-radical (Zhou 2020) or free-radical interventions through creating ion-pairs, and inner-sphere nature intermediate complexes (Glebov et al. 2011). Absent free-radical intervention certain reactions of oxidation were carried out via outer-sphere mechanisms (Matyjaszewski 1998).

Considering the above discrepancies between the kinetic outcome and those for other polysaccharides oxidized by this oxidant, all reactants with a more aggressive permanganic acid ($HMnO_4$) and alkoxinium ion ($BTBH^+$) are protonated in the most possible reaction pathway that may be proposed to oxidize BTB by permanganate ion [H^+], [substrate], and ionic strength depending on the reaction specimen indicate that the most suitable reaction mechanism for oxidation triggered by both [BTB] and MnO_4^-.

$$BTB + H^+ \overset{K_1}{\rightleftharpoons} BTBH^+ \tag{2}$$

$$MnO_4^- + H^+ \overset{K_2}{\rightleftharpoons} HMnO_4 \tag{3}$$

The $[BTBH]^+$ a substrate, with proton release before the speed determinant stage, was followed by an $HMnO_4$ attack at the centre of a 1:1 intermediate complex (C_1).

$$HMnO_4 + BTBH^+ \overset{K_3}{\rightleftharpoons} C_1 + H^+. \tag{4}$$

Instead, in a rate-determining stage, the slow decomposition of the formed intermediate complex to give radical (C_1.) substrate and reduced (Red) shape (as Mn^{III}/Mn^{IV}) of the permanganate ion, throughout the slow stage first oxidation products as follows.

$$C_1 \longrightarrow kC_1^{\cdot} + \text{Red}. \tag{5}$$

Under pseudo first-order conditions used, the change of the rate constants with changing the [H^+] and [BTB] and rearrangement, the following relationship is obtained,

$$\frac{[BTB]}{k_{obs}} = \frac{1}{k_n} = \left(\frac{[H^+]^{-1}}{k'} + \frac{1}{k''}\right) \tag{6}$$

where k_n is the second-order rate constant, $k` = kK_1K_2K_3$ and $k'' = kK_2K_3$, respectively. In compliance with Eq. (6) $[BTB]/k_{Obs}$ versus $[H^+]^{-1}$ has given good straight lines with a positive intercept on $[BTB]/k_{obs}$ axes, as shown in Fig. 5; the values of the apparent rate constants k', k'' and the protonation constant K_1 can be determined on their slopes and

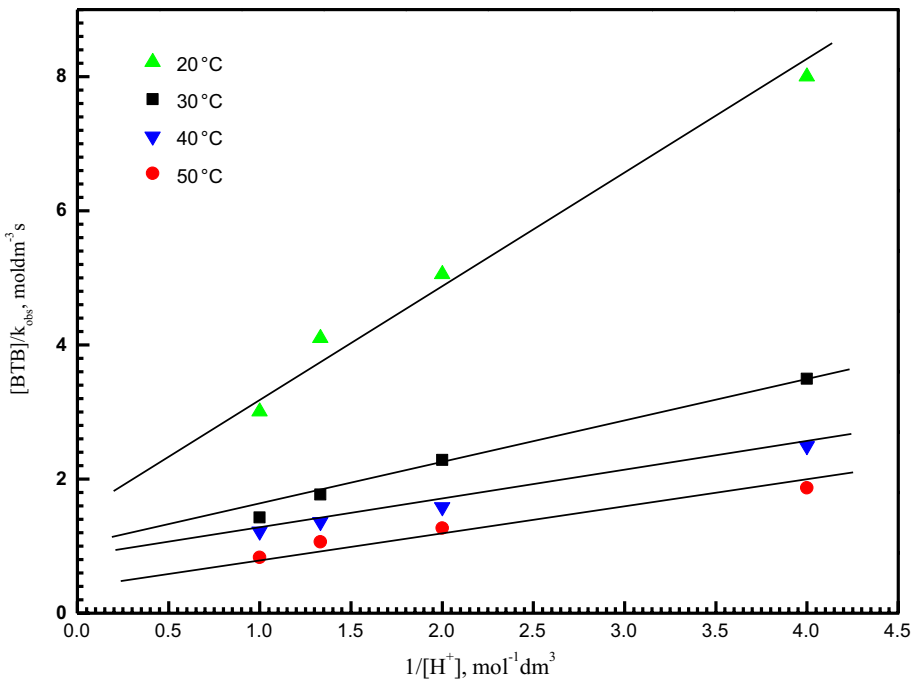

Fig. 5 Plots of $[BTB]/k_{obs}$ vs $1/[H^+]$ in the oxidation of bromothymol blue by permanganate ion in aqueous perchlorate solutions. $[MnO_4^-] = 4.0 \times 10^{-4}$, $[BTB] = 1.0 \times 10^{-3}$, $I = 1.0$ mol dm^{-3} at various temperatures

intercepts. These values were determined to utilize the least square method and found at 20, 30, 40 and 50 °C, respectively, to be 0.91, 0.79, 0.57 and 0.55. It was observed that, the measured values of the protonation constants (K_1) are in strong agreement.

The negative entropies of activation ($\Delta S^{\neq}$) values in Table 1 show the density of the intermediates rather than the reactants. Again, the values of positive for $\Delta G^{\neq}$ indicated that the intermediate complexes produced were non-spontaneity as suggested by the proposed mechanism. As shown by the ionic strength dependency of the rate constant, the strong reaction propensity between the neutral molecule and the positive ion will support the low energy activation value of $E^{\neq}$ (Table 1) observed in this step. It implies that the reactants need little energy to interact and create the intermediate states of the complexes developed.

However, the entropy of activation has been previously reported (Hassan 1992, 2011) as being more negative for inner reactions, with reactions with negative values of the $\Delta S^{\neq}$ being conducted through an inner-sphere of one- and two-electron transfer mechanism. Considering the values found for the entropy of activities (Table 1), it is better to use permanganate ion to oxidize BTB by means of two-electron shifts within the sphere rather than by the outside-sphere method. It should be remembered in this context that the mechanism of outer-sphere two-electron transition does not seem to be experimentally confirmed.

The disturbance of the alteration in spectra (Fig. 1) can suggest that the original quick portion of the reaction to oxidation is not the true phase of electron transfer. Therefore, the quick development of an intermediate between the reactants can be due to the first strong portion of the oxidation. Once again, several trials were conducted to detect the formation of intermediate hypomanganate (V) as transient species. Unfortunately, all attempts were unsuccessful. Under our experimental conditions of lower concentrations of reactants or the rapid reaction between the formulated Mn(V) and Cr, this failure may be due to the lower absorptivity of formed Mn(V). Equation 5 defining the final products for oxidation. In view of the above-mentioned kinetic definitions and study results, as outlined in Scheme 1, a tentative reaction process can be proposed for oxidation of bromothymol blue by acidic permanganate.

Energy gap

From Fig. 1, Spectral changes of wavelength 200 nm < λ < 900 nm in the oxidation of [BTB] by permanganate ion in aqueous $HClO_4$ during the reaction progression to obtained $[BTB]^{Keto}$. The optical transitions occur by direct transitions in semiconductor materials (Cong et al. 2020). At incident photons energy ($h\upsilon$), the $(\alpha h\upsilon)^m = B\left(h\upsilon - E_g\right)$ the equation may be used to obtain optical band gap $\left(E_g^{Opt}\right)$ and transition bandgap (E_g^{trans}) values according to *Tauc's*

Table 1 The constant of protonation (K_1) and the values of the apparent rate constants ($k`$ and k'') in the oxidation of [BTB] by $\left[MnO_4^-\right]$ in aqueous $HClO_4$ solutions

Constants	Parameter			
	$\Delta H^{\neq}$ kJ mol^{-1}	$\Delta S^{\neq}$ J mol^{-1} K^{-1}	$\Delta G^{\neq}{}_{293}$ kJ mol^{-1}	$E_a^{\neq}$ kJ mol^{-1}
k'	43.66	− 391.09	114.63	50.36
k''	18.14	− 305.96	89.66	26.96
$^{a}k_n`$	21.35	− 181.25	53.13	23.95
	$\Delta H°$ kJ mol^{-1}	$\Delta S°_{293}$ J mol^{-1} K^{-1}	$\Delta G°_{293}$ kJ mol^{-1}	
K_1	− 12.49	− 0.0433	+ 0.219	

Errors of experimental ± 4%, *a*: The constant of second-order rate at $[H^+] = 0.5$ mol dm^{-3}

Scheme 1 Mechanism of oxidation of bromothymol blue by permanganate ion in aqueous perchlorate solutions

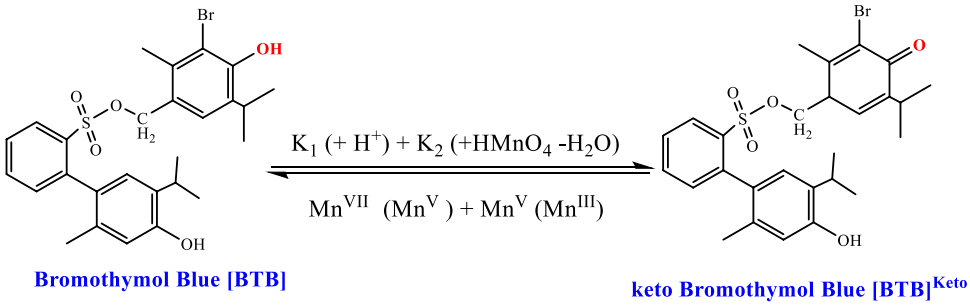

Bromothymol Blue [BTB] **keto Bromothymol Blue $[BTB]^{Keto}$**

equation from the optical transition spectrum, where $m=2$ for direct transitions allowed spectrum, respectively. They allow direct transitions of [BTB] and $[BTB]^{Keto}$ are shown in Fig. 6. Extrapolating the right part of the plot $(\alpha h\nu)^2$ to the energy axis at $\alpha=0$ in addition to $(h\nu)$ obtains the optical gap values. Figure 6 displays the $(\alpha h\nu)^2\times10^{12}$ $(eVm^{-1})^2$ versus $h\nu$ (eV) (Al-Hossainy et al. 2017; Rammah et al. 2019). The meaning $\left(E_g^{Opt}\right)$ is described as the lower part of the energy, or a pair of bound electron–hole generators assigned to Frankel's exciton. The meaning $\left(E_g^{Opt}\right)$ applies to the disparity between LUMO and HOMO in the energy value (Awad et al. 2004).

Application of Tauc's equation, the results clearly display that the values of the optical energy bandgap $\left(E_g^{Opt}\right)$ direct transition decreases from 2.849 eV for [BTB] to 2.35 eV for $[BTB]^{Keto}$. The various between the $\left(E_g^{Opt}\right)$ of [BTB] to $[BTB]^{Keto}$ thin film is 0.499 eV. This indicates that $[BTB]^{Keto}$ (result from oxidation process) integrates the energy levels into the bandgap, which reduces the energy gap value. In DFTs simulation section by utilizing $DMol^3$, the $\left(E_g^{Opt}\right)$ values for [BTB] and $[BTB]^{Keto}$ are 3.047 eV and 2.869 eV, respectively (Nayeri et al. 2014; Al-Hossainy et al. 2019b). It can also be noted that the HOMO and LUMO simulation is shown in inset Fig. 6 indicates the average similarity of the energy gap values calculated by Tauc's equation with a small difference in values.

Molecular electrostatic potential (MEP) and potential (P)

[BTB] and $[BTB]^{Keto}$ chemical and physical comparisons were tested using the electron density and the electrostatic potential. For the [BTB] and $[BTB]^{Keto}$, the electron density is often discussed as the essential factor in determining the ground state of a significant number of electron systems. Based on the constant electron density, the MEP defines electrostatic potential. A 3D diagram reveals the active position of the MEP in Fig. 7a, c respectively for [BTB] and $[BTB]^{Keto}$. The color blue is the appropriate zone for nuclear attacks, whereas the appropriate zone for electrophilic attacks is a color red. In the isolated molecule and crystal models the range molecular electrostatic potential of [BTB] and $[BTB]^{Keto}$ is $-5.929\times10^{-2}\geq[MEP]\geq5.929\times10^{-2}$, and in the order of increase is $-6.838\geq[MEP]\geq6.838$ in volume, respectively: red < brown < blue (Cruz et al. 2019; Kumar et al. 1996). The largest attraction is the blue color, while the red color one seems to have a strong repudiation. The MEP graph indicates (Abdel-Aziz et al. 2018) that electron-negative nitrogen atoms represent negative potential regions and that positive potential is present in the hydrogen atoms (Al-Hossainy et al. 2019c). The potential possible diagrams (Fig. 7b, d), the potential growth of [BTB] is shown to be lower than that of $[BTB]^{Keto}$. This shows the electron transfer probabilities (Hassan et al. 2009c; Li et al. 2020; Al-Hossainy et al. 2019d) in $[BTB]^{Keto}$ are increased.

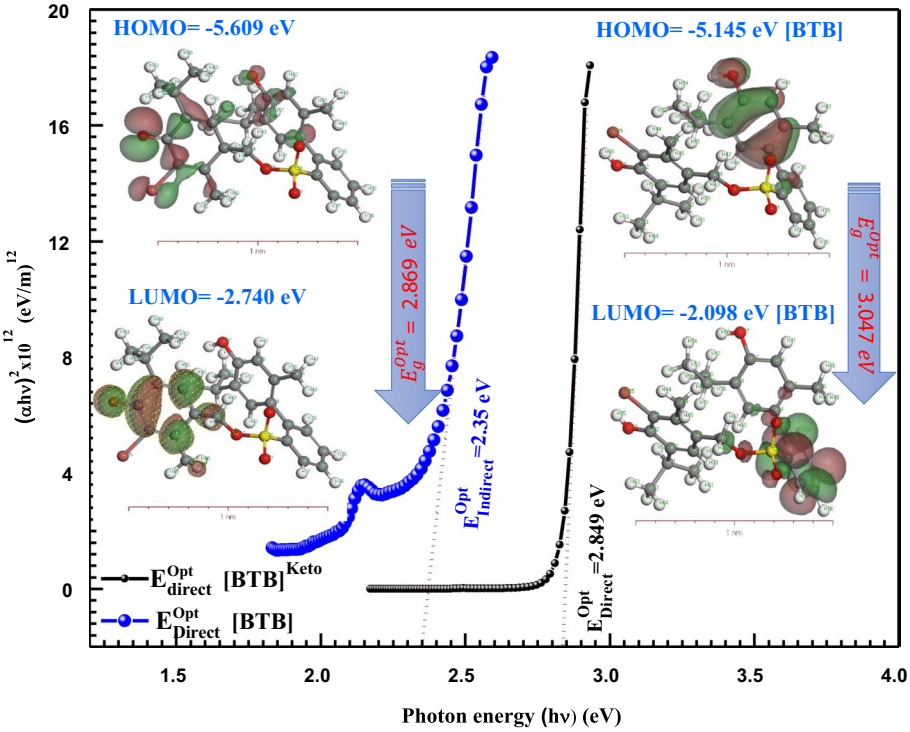

Fig. 6 Experimental plot of $(\alpha h\nu)^2$ versus photon energy $(h\nu)$ for [BTB] and $[BTB]^{Keto}$. Inset this figure HOMO and LUMO for the [BTB] and $[BTB]^{Keto}$ using DFT/CASTEP program

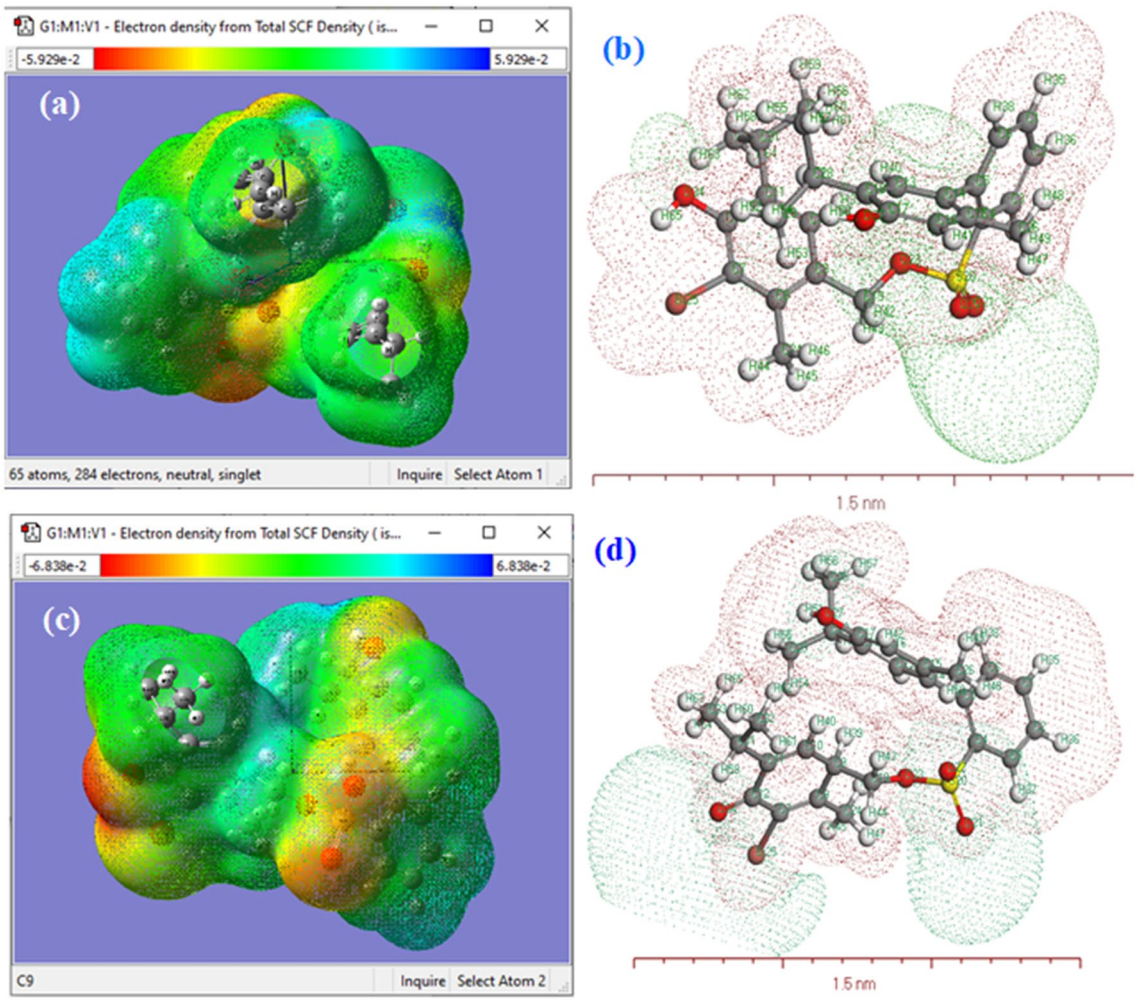

Fig. 7 **a** MEP of [BTB]; **b** potential of [BTB]; **c** MEP of $[BTB]^{Keto}$ and **d** potential of $[BTB]^{Keto}$ by use the *material studio and Gaussian program* calculation DFT

Conclusions

The significant structural characteristics, optical dispersion and dielectric properties of [BTB] and $[BTB]^{Keto}$ are determined using FTIR technique and compared with DFT calculations. The simulated FTIR (*Gaussian DFT*) of [BTB] and $[BTB]^{Keto}$ in isolated and gas state are in great agreement for the same compounds obtained from experimental analyses. The kinetics and oxidation processes of BTB in acid perchlorate solutions with a constant ionic strength of 1.0 mol dm^{-3} as sulfonphthaleine dyes by permanganate ion oxidizer have been analyzed spectrophotometrically. The experimental results of the pseudo-first-order plots revealed that oxidation displays a single pathway reaction; MnO_4^- first-order, [BTB] fractional-first order and hydrogen ion concentration fractional-first order. Dependence on acidity in reaction levels suggested acid-catalyzed reaction. The addition of Mn^{II} to the reaction mixtures confirmed the absence of either Mn^{III} and/or Mn^{IV} transient species as involvement species in the oxidation phase. Formation of 1:1 intermediate complex prior to the rate-determining step was revealed, kinetically. A tentative method of the reaction was introduced and discussed with respect to the kinetic observations and measured kinetic parameters. The E_g^{Opt} values achieved from Tauc's equation are 2.849 eV and 2.35 eV for [BTB] and $[BTB]^{Keto}$ respectively. While the E_g^{Opt} computed by DFT ($DMol^3$) are 3.047 eV and 2.869 eV for [BTB] and $[BTB]^{Keto}$ as—isolated and gas state, respectively. There is a good agreement between E_g^{Opt} values determined by the DFT ($DMol^3$) computations and the Tauc's equation calculations. Based on the E_g^{Opt} values and DFT calculation ($E_{HOMO} - E_{LUMO}$) of [BTB] and $[BTB]^{Keto}$ can be used as an application to textile industrial wastewater treatment.

Compliance with ethical standards

Conflict of interest The authors declare that they have no known competing financial interests or personal relationships that could have appeared to influence the work reported in this paper.

References

Abbasi A, Sardroodi JJ (2016) N-doped TiO_2 anatase nanoparticles as a highly sensitive gas sensor for NO_2 detection: insights from DFT computations. Environ Sci Nano 3(5):1153–1164

Abdel-Aziz M, Al-Hossainy AF, Ibrahim A, El-Maksoud SA, Zoromba MS, Bassyouni M, Abdel-Hamid S, Abd-Elmageed A, Elsayed I, Alqahtani O (2018) Synthesis, characterization and optical properties of multi-walled carbon nanotubes/aniline-o-anthranilic acid copolymer nanocomposite thin films. J Mater Sci Mater Electron 29(19):16702–16714

Abdel-Aziz M, Zoromba MS, Bassyouni M, Zwawi M, Alshehri A, Al-Hossainy AF (2020) Synthesis and characterization of Co-Al mixed oxide nanoparticles via thermal decomposition route of layered double hydroxide. J Mol Struct 1206:127679

Abdel-Hamid M, Khairou K, Hassan R (2003) Kinetics and mechanism of permanganate oxidation of pectin polysaccharide in acid perchlorate media. Eur Polymer J 39(2):381–387

Abd-Elmageed A, Al-Hossainy AF, Fawzy E, Almutlaq N, Eid M, Bourezgui A, Abdel-Hamid S, Elsharkawy N, Zwawi M, Abdel-Aziz M (2020) Synthesis, characterization and DFT molecular modeling of doped poly (para-nitroaniline-co-para-toluidine) thin film for optoelectronic devices applications. Opt Mater 99:109593

Al-Hossainy AF, Zoromba MS (2019) Doped-poly (para-nitroaniline-co-aniline): synthesis, semiconductor characteristics, density, functional theory and photoelectric properties. J Alloy Compd 789:670–683

Al-Hossainy AF, Mohamed AE, Hassan FS, Allah MA (2017) Determination of cadmium and lead in perch fish samples by differential pulse anodic stripping voltammetry and furnace atomic absorption spectrometry. Arab J Chem 10:S347–S354

Al-Hossainy AF, Abd-Elmageed A, Ibrahim ATA (2019a) Synthesis, structural and optical properties of gold nanoparticle-graphene-selenocysteine composite bismuth ultrathin film electrode and its application to Pb(II) and Cd (II) determination. Arab J Chem 12(8):2853–2863

Al-Hossainy AF, Ibrahim A, Zoromba MS (2019b) Synthesis and characterization of mixed metal oxide nanoparticles derived from Co–Cr layered double hydroxides and their thin films. J Mater Sci Mater Electron 30(12):11627–11642

Al-Hossainy AF, Zoromba MS, El-Gammal O, El-Dossoki FI (2019c) Density functional theory for investigation of optical and spectroscopic properties of zinc-quinonoid complexes as semiconductor materials. Struct Chem 30(4):1365–1380

Al-Hossainy AF, Zoromba MS, Abdel-Aziz M, Bassyouni M, Attar A, Zwawi M, Abd-Elmageed A, Maddah H, Slimane AB (2019d) Fabrication of heterojunction diode using doped-poly (ortho-aminophenol) for solar cells applications. Physica B 566:6–16

Awad IM, Hassan FS, Mohamed AE, Al-Hossainy AF (2004) Diphosphine compounds: part I. Novel biologically active 1, 1′ bis-AND/OR 1, 2-cis-(diphenylphosphino-) ethene and their complexes [M (CO) n {Ph2P (CHn) nPPh2}] & [Cu (Cl) 2 {Ph2P (CHn) nPPh2}],(M = W, Mo, Crn = 1, 2…. n). Phosphorus Sulfur Silicon 179(7):1251–1266

Badeenezhad A, Azhdarpoor A, Bahrami S, Yousefinejad S (2019) Removal of methylene blue dye from aqueous solutions by natural clinoptilolite and clinoptilolite modified by iron oxide nanoparticles. Mol Simul 45(7):564–571

Bahar MM, Mahbub KR, Naidu R, Megharaj M (2020) A simple spectrophotometric method for rapid quantitative screening of arsenic bio-transforming bacteria. Environ Technol Innov 19:100840

Bourezgui A, Kacem I, Daoudi M, Al-Hossainy AF (2020) Influence of gamma-irradiation on structural, optical and photocatalytic performance of TiO_2 nanoparticles under controlled atmospheres. J Electron Mater 49(3):1904–1921

Cong C, Shang J, Chen Y, Shan Y, Yu T (2020) Optical characterization of two-dimensional semiconductors. In: Chi D, Goh KJ, Wee AT (eds) 2D semiconductor materials and devices. Elsevier, Amsterdam, pp 135–166

Cruz JC, Hernández-Esparza R, Vazquez-Mayagoitia A, Vargas R, Garza J (2019) Implementation of the molecular electrostatic potential over graphics processing units. J Chem Inf Model 59(7):3120–3127

Farzaneh A, Esrafili MD, Mermer Ö (2020) Development of TiO_2 nanofibers based semiconducting humidity sensor: adsorption kinetics and DFT computations. Mater Chem Phys 239:121981

Gao J-F, Duan W-J, Zhang W-Z, Wu Z-L (2020) Effects of persulfate treatment on antibiotic resistance genes abundance and the bacterial community in secondary effluent. Chem Eng J 382:121860

Glebov EM, Pozdnyakov IP, Grivin VP, Plyusnin VF, Zhang X, Wu F, Deng N (2011) Intermediates in photochemistry of Fe(III) complexes with carboxylic acids in aqueous solutions. Photochem Photobiol Sci 10(3):425–430

Gunter TE, Gerstner B, Lester T, Wojtovich AP, Malecki J, Swarts SG, Brookes PS, Gavin CE, Gunter KK (2010) An analysis of the effects of Mn2+ on oxidative phosphorylation in liver, brain, and heart mitochondria using state 3 oxidation rate assays. Toxicol Appl Pharmacol 249(1):65–75

Hassan RM (1992) The oxidation of uranium (IV) by polyvalent metal ions. A linear free-energy correlation. J Coord Chem 27(4):255–266

Hassan RM (1993) Alginate polyelectrolyte ionotropic gels. XIV. Kinetics and mechanism of formation of intermediate complex during the oxidation of alginate polysaccharide by alkaline permanganate with a spectrophotometric evidence of manganate (VI) transient species. J Polym Sci Part A Polym Chem 31(1):51–59

Hassan RM (2011) A mechanistic approach to the kinetics of oxidation of uranium (IV) by hexachloroplatinate (IV) in aqueous perchlorate solutions. Evidence of the formation of a binuclear intermediate complex. J Phys Chem A 115(46):13338–13345

Hassan RM (2020) Prospective mechanistic on electron-transfer nature for reduction of permanganate ion by ascorbic acid in aqueous acidic solutions. J Mol Liq 309:113154

Hassan R, Ibrahim SM (2019a) Kinetics and mechanism of permanganate oxidation of ADA in aqueous perchlorate solutions. Curr Organocatal 6(1):52–60

Hassan RM, Ibrahim SM (2019b) Oxidation of some sustainable sulfated natural polymers: kinetics and mechanism of oxidation of water-soluble chondroitin-4-sulfate polysaccharide by hexachloroiridate(IV) in aqueous solutions. ACS Omega 4:2463–2471

Hassan RM, Abdel-Kader DA, Ahmed SM, Fawzy A, Zaafarany IA, Asghar BH, Takagi HD (2009a) Acid-catalyzed oxidation of carboxymethyl cellulose. Kinetics and mechanism of permanganate oxidation of carboxymethyl cellulose in acid perchlorate solutions. Catal Commun 11(3):184–190

Hassan R, Fawzy A, Ahmed G, Zaafarany I, Asghar B, Khairou K (2009b) Acid-catalyzed oxidation of some sulfated macromolecules. Kinetics and mechanism of oxidation of kappa-carrageenan polysaccharide by permanganate ion in acid perchlorate solutions. J Mol Catal A Chem 309(1–2):95–102

Hassan FS, Al-Hossainy AF, Mohamed AE (2009c) Diphosphine compounds, part III: UV/Visible spectroscopy and novel routes to functionalized diphosphine-M (CO) 6 complexes (M = W, Mo, or Cr). Phosphorus Sulfur Silicon 184(11):2996–3022

Hassan R, Fawzy A, Alarifi A, Ahmed G, Zaafarany I, Takagi H (2011) Base-catalyzed oxidation of some sulfated macromolecules: kinetics and mechanism of formation of intermediate complexes of short-lived manganate (VI) and/or hypomanganate (V) during oxidation of iota-and lambda-carrageenan polysaccharides by alkaline permanganate. J Mol Catal A Chem 335(1–2):38–45

Hassan R, Dahy AR, Ibrahim S, Zaafarany I, Fawzy A (2012) Oxidation of some macromolecules. Kinetics and mechanism of oxidation of methyl cellulose polysaccharide by permanganate ion in acid perchlorate solutions. Ind Eng Chem Res 51(15):5424–5432

Hassan RM, Ibrahim SM, Dahy AA, Zaafarany IA, Tirkistani F, Takagi HD (2013) Kinetics and mechanism of oxidation of chondroitin-4-sulfate polysaccharide by chromic acid in aqueous perchlorate solutions. Carbohyd Polym 92:2321–2326

Hassan R, Ibrahim S, Sayed S (2018a) Kinetics and mechanistic aspects on electron-transfer process for permanganate oxidation of poly (ethylene glycol) in aqueous acidic solutions in the presence and absence of Ru (III) catalyst. Int J Chem Kinet 50(11):775–783

Hassan RM, Ibrahim SM, Khairou KS (2018b) Kinetics and mechanism of oxidation of pyruvate by permanganate ion in aqueous perchlorate solution. Transit Met Chem 43:683–691

Hassan RM, Ibrahim SM, Khairou KS (2019) Novel synthesis of diketopectate coordination biopolymer derivatives as alternative promising in biomedicine, pharmaceutics and food Industrial applications. J Nutr Food Process 2:1–5

Hassan R, Takagi H, Ibrahim S (2020a) Orientation on the mechanistics of electron-transfer on oxidation of chondroitin-4-sulfate as sustainable sulfated polysaccharide by permanganate ion in aqueous perchlorate solutions. J Renew Mater 8(2):205–218

Hassan RM, Ibrahim SM, Sayed SA, Zaafarany IA (2020b) Promising iocompatible, biodegradable, and inert polymers for purification of wastewater by simultaneous removal of carcinogenic Cr(VI) and present toxic heavy metal cations: reduction of chromium(VI) by poly(ethylene glycol) in aqueous perchlorate solutions. ACS Omega 5:4424–4432

Hicks KW (1976) Kinetics of the permanganate ion-potassium octacyanotungstate(IV) reaction. J Inorg Nucl Chem 38:1381–1383

Ibrahim SM, Althagafi I, Takagi HD, Hassan RM (2017) Kinetics and mechanism of oxidation of chondroitin-4-sulfate polysaccharide as a sulfated polysaccharide by hexacyanoferrate(III) in alkaline solutions with synthesis of novel coordination biopolymer chelating agent. J Mol Liq 244:353–359

Ibrahim SM, Bourezgui A, Abd-Elmageed A, Kacem I, Al-Hossainy AF (2020) Structural and optical characterization of novel [ZnKCMC] TF for optoelectronic device applications. J Mater Sci Mater Electron 31:8690–8704

Khairou K, Hassan R (2000) Pectate polyelectrolyte ionotropic gels: 1. Kinetics and mechanisms of formation of manganate (VI)–pectate intermediate complex during the oxidation of pectate polysaccharide by alkaline permanganate. Eur Polym J 36(9):2021–2030

Khan S, Malik A (2014) Environmental and health effects of textile industry wastewater, Environmental deterioration and human health. Springer, Berlin, pp 55–71

Knežević M, Kramar A, Hajnrih T, Korica M, Nikolić T, Žekić A, Kostić M (2020) Influence of potassium permanganate oxidation on structure and properties of cotton. J Nat Fibers. https://doi.org/10.1080/15440478.2020.1745120

Kumar A, Mohan CG, Mishra P (1996) Molecular electrostatic potential and field as descriptors of hydrogen bonding and molecular activity. Effects of hybridization displacement charge. J Mol Struct 361(1–3):135–144

Laidler K (1965a) Chemical kinetics. McGraw-Hill, New York

Laidler K (1965b) The analysis of kinetic results, chemical kinetics. McGraw-Hill Inc, New York, pp 19–21

Li Y, Wang Y, Song K, Liu L, Cai R, Tao G, Zhao P, Zhou H, He H (2018) A rapid and sensitive colorimetric assay for the determination of adenosine kinase activity. Biochem Biophys Res Commun 502(2):250–254

Li D, Gao J, Cheng P, He J, Yin Y, Hu Y, Chen L, Cheng Y, Zhao J (2020) 2D boron sheets: structure, growth, and electronic and thermal transport properties. Adv Func Mater 30(8):1904349

Liu S, Salhi E, Huang W, Diao K, von Gunten U (2019) Kinetic and mechanistic aspects of selenite oxidation by chlorine, bromine, monochloramine, ozone, permanganate, and hydrogen peroxide. Water Res 164:114876

Manhas MS, Mohammed F (2007) A kinetic study of oxidation of β-cyclodextrin by permanganate in aqueous media. Colloids Surf A 295(1–3):165–171

Matyjaszewski K (1998) Inner sphere and outer sphere electron transfer reactions in atom transfer radical polymerization. In: Macromolecular symposia, Wiley Online Library, pp 105–118

Mollan TL, Alayash AI (2013) Redox reactions of hemoglobin: mechanisms of toxicity and control. Mary Ann Liebert, Inc, New Rochelle

Nayeri FD, Karegar F, Kolahdouz M, Asl-Soleimani E (2014) Low temperature insertion of energy levels into the ZnO nanorod's bandgap by nanotube conversion. Thin Solid Films 562:343–346

Pavitha P, Prashanth J, Ramu G, Ramesh G, Mamatha K, Reddy BV (2017) Synthesis, structural, spectroscopic, anti-cancer and molecular docking studies on novel 2-[(Anthracene-9-ylmethylene) amino]-2-methylpropane-1, 3-diol using XRD, FTIR, NMR, UV–Vis spectra and DFT. J Mol Struct 1147:406–426

Radhakrishnamurti P, Rao M (1977) Oxidation of aliphatic ketones, substituted acetophenones & cyclic ketones by potassium permanganate

Rammah Y, Ali A, El-Mallawany R, Abdelghany A (2019) Optical properties of bismuth borotellurite glasses doped with NdCl3. J Mol Struct 1175:504–511

Rashid TU, Kabir SF, Biswas MC, Bhuiyan MR (2020) Sustainable wastewater treatment via dye–surfactant interaction: a critical review. Ind Eng Chem Res 59:9719–9745

Rauf M, Hisaindee S, Saleh N (2015) Spectroscopic studies of keto–enol tautomeric equilibrium of azo dyes. RSC Adv 5(23):18097–18110

Saini RD (2017) Textile organic dyes: polluting effects and elimination methods from textile waste water. Int J Chem Eng Res 9:975–6442

Shaker AM (2001) Base-catalyzed oxidation of carboxymethyl-cellulose polymer by permanganate: 1. Kinetics and mechanism of formation of a manganate (VI) transient species complex. J Colloid Interface Sci 233(2):197–204

Shaker AM, El-Khatib RM, Mahran HS (2007) Kinetics and mechanism of the decay of methyl cellulose-manganate (VI) polysaccharide transient species–novel spectrophotometric kinetic trace of methyl cellulose hypomangate (V) gel intermediate polysaccharide. J Appl Polym Sci 106(4):2668–2674

Srebro M, Govind N, De Jong WA, Autschbach J (2011) Optical rotation calculated with time-dependent density functional theory: the OR45 benchmark. J Phys Chem A 115(40):10930–10949

Surowka AD, Birarda G, Szczerbowska-Boruchowska M, Cestelli-Guidi M, Ziomber-Lisiak A, Vaccari L (2020) Model-based correction algorithm for Fourier Transform Infrared microscopy measurements of complex tissue-substrate systems. Anal Chim Acta 1103:143–155

Tandon PK, Mehrotra A, Shrivastava M, Dhusia M, Singh SB (2007) Ru (III) catalysis in the reaction of hexacynoferrate (III) and iodide ions in perchloric acid medium. Transit Met Chem 32:991–999

Thabet HK, Al-Hossainy AF, Imran M (2020) Synthesis, characterization, and DFT modeling of novel organic compound thin films derived from 2-amino-4-(2-hydroxy-3-methoxyphenyl)-4H-thiazolo [3, 2-a][1, 3, 5] triazin-6 (7H)-one. Opt Mater 105:109915

Tittmann K (2009) Reaction mechanisms of thiamin diphosphate enzymes: redox reactions. FEBS J 276(9):2454–2468

Wasserman MR, Alejo JL, Altman RB, Blanchard SC (2016) Multiperspective smFRET reveals rate-determining late intermediates of ribosomal translocation. Nat Struct Mol Biol 23(4):333

Xu X-R, Li H-B, Wang W-H, Gu J-D (2005) Decolorization of dyes and textile wastewater by potassium permanganate. Chemosphere 59(6):893–898

Xu X, Chen R, Pan R, Zhang D (2020) Pyrolysis kinetics, thermodynamics and volatiles of representative pine wood with thermogravimetry/Fourier transform infrared analysis. Energy Fuels 34:1859–1869

Zaafarany I, Gobouri A, Hassan R (2013) Oxidation of some sulfated carbohydrates: kinetics and mechanism of oxidation of chondroitin-4-sulfate by alkaline permanganate with novel synthesis of coordination biopolymer precursor. J Mater Sci Res 2(4):23

Zhou D (2020) Impact of exercise training on free radical metabolism of myocardium, quadriceps and liver in mice. Revista Cientifica-Facultad de Ciencias Veterinarias 30(3)

Zoromba MS, Al-Hossainy AF (2020) Doped poly (o-phenylenediamine-co-p-toluidine) fibers for polymer solar cells applications. Sol Energy 195:194–209

Zoromba MS, Abdel-Aziz M, Bassyouni M, Bahaitham H, Al-Hossainy AF (2018) Poly (o-phenylenediamine) thin film for organic solar cell applications. J Solid State Electrochem 22(12):3673–3687

Affiliations

Samia M. Ibrahim[1] · Ahmed F. Al-Hossainy[1,2]

✉ Samia M. Ibrahim
samiamakram2001@yahoo.com

✉ Ahmed F. Al-Hossainy
ahmed73chem@scinv.au.edu.eg

[1] Chemistry Department, Faculty of Science, New Valley University, El-Kharga 72511, New Valley, Egypt

[2] Chemistry Department, Faculty of Science, Northern Border University, Arar 1321, Saudi Arabia